Slow Slip Events in the Kanto and Tokai Regions of Central Japan Detected Using Global Navigation Satellite System Data During 1994–2020

Takuya Nishimura[1] (ORCID)

[1]Disaster Prevention Research Instutite, Kyoto University, Kyoto, Japan

Abstract Slow slip events (SSEs) along subduction zones play an important role in accommodating relative plate motion. SSEs interplay with large megathrust earthquakes and other slow earthquakes, including low frequency and very low frequency earthquakes. The Kanto and Tokai regions of central Japan host frequent slow and large earthquakes, with significant differences in slip behavior along the subduction zones in the Suruga Trough, Sagami Trough, and Japan Trench. In this study, we conducted a systematic search to estimate the fault models and durations of short-term SSEs using continuous Global Navigation Satellite System data collected from 1994 to 2020. We detected 176 potential SSEs with moment magnitudes of 5.3–7.0 and durations of 0–80 days from the time series. Along the Sagami Trough, two shallow regions at a depth of 10–20 km host $M_w \geq 6.5$ SSEs off of the Boso Peninsula and accommodate most of the relative plate motion aseismically. Some SSEs also occur on the deep plate interface down to ~50 km without tectonic tremors. Along the Japan Trench, the cumulative slip of the SSEs exhibits a bimodal depth distribution to avoid the large slip areas of past megathrust earthquakes at 30–40 km depth. The shallow SSEs are in the same depth range (10–30 km) as tectonic tremors, but are spatially separate from tremors along the trench. The detected SSEs have limited temporal correlations with other slow earthquakes and earthquake swarms, which suggests that many factors control the genesis of slow and regular earthquakes.

1. Introduction

A slow slip event (SSE) is a transient slip phenomenon that releases elastic strain around a fault. SSEs have been detected using geodetic techniques in the last few decades (e.g., Schwartz & Rokosky, 2007). Detecting SSEs is essential for answering scientific questions, including what controls the occurrence of an SSE, that is, geometric, mechanical, frictional, hydrologic, metamorphic, and thermal conditions in the fault zone (e.g., Ikari et al., 2013; S. W. Ozawa et al., 2019; Saffer & Wallace, 2015). However, detecting SSEs is still challenging because the small transient signal related to an SSE is often buried in noisy data. Previous studies have proposed various methods to detect the faint surface displacement caused by an SSE (e.g., Haines et al., 2019; Nishimura et al., 2013; Rousset et al., 2017; Takagi et al., 2019). These observations can help determine the mechanism that produces SSEs, as well as understanding the interplay between SSEs and regular earthquakes. SSEs can trigger a large earthquake (e.g., Ito et al., 2013; Radiguet et al., 2016) or numerous small swarms of earthquakes (e.g., Nishikawa & Ide, 2018; Vallée et al., 2013). SSEs accommodate a significant part of relative plate motion (e.g., Bartlow, 2020; Nishimura et al., 2013; Radiguet et al., 2016; Wallace, 2020) and may act as a barrier of rupture propagation of megathrust earthquakes (Nishikawa et al., 2019). Large earthquakes can also modulate SSE activity (e.g., H. Hirose et al., 2012; Wallace, 2020; Yarai & Ozawa, 2013). The Kanto region of central Japan is one of the best places to study this type of interplay with high-quality geodetic data because of large (up to M ~9) megathrust earthquakes and frequent SSEs that are known to occur in the region.

The elevated seismicity in the Kanto region is attributed to its complex tectonic setting, where two oceanic plates subduct from the south and east (Figure 1 and Figure S1). More than 200 M ≥6 earthquakes have been instrumentally recorded in the Kanto region in the past century, including the surrounding offshore region. Major cities, including Tokyo and Yokohama, in the southern part of the Kanto region were heavily damaged by the 1923 M_w 7.9 Kanto earthquake, which occurred at the interface between the overriding continental plate and the subducting Philippine Sea plate in the Sagami Trough (e.g., Pollitz et al., 2005). West
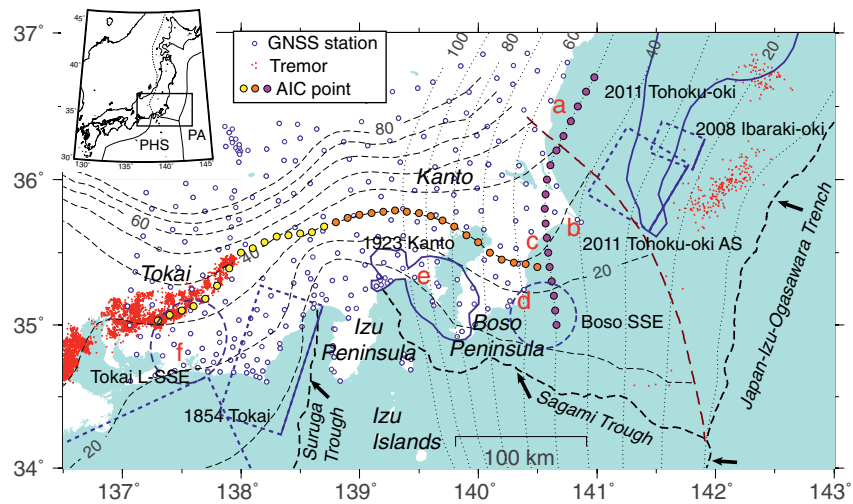
Figure 1. Map of the study area. Dashed and dotted contours are iso-depths of the plate interfaces for the Philippine Sea plate (PHS) and the Pacific plate (PA), respectively. Arrows near the trenches and troughs represent approximate directions of relative block motion (Nishimura et al., 2018). Blue circles indicate GNSS stations. The stations labeled a–f correspond to parts of Figure 2, showing the coordinate time series. Yellow, orange, and magenta circles indicate the central points of the rectangular areas used to calculate ΔAIC averages of the N40°W, N25°W, and N80°W components, respectively. Red dots indicate tectonic tremors (Nishikawa et al., 2019; Obara et al., 2010). Source regions for the 1923 M_w 7.9 Kanto earthquake and the 2011 M_w 9.0 Tohoku-oki earthquake show 2 m (Pollitz et al., 2005) and 5 m (S. Ozawa et al., 2012) contours of coseismic slip, respectively. Rectangular fault models for the largest M_w 7.8 aftershock of the Tohoku-oki earthquake (Nishimura et al., 2011), the 2008 M_w 6.8 Ibaraki-oki earthquake (GSI, 2008), and the 1854 M_w 8.0 Ansei-Tokai earthquake (Ishibashi, 1981) are also shown. (Inset) Regional tectonic map of the study area. AIC, Akaike Information Criterion; GNSS, Global Navigation Satellite System.

of the Sagami Trough, the Philippine Sea plate collides with the Honshu arc at the base of the Izu Peninsula and subducts beneath the Tokai region in the Suruga Trough. The 1854 M_w 8.0 Ansei-Tokai earthquake ruptured the megathrust along the Suruga Trough, which is the easternmost part of the Nankai Trough (e.g., Ishibashi, 1981). No deep seismicity related to the subducting Philippine Sea plate is observed north of the collision zone between these two troughs (Ishida, 1992). The directions of relative plate convergence differ significantly along the two troughs due to strain partitioning within the subducting Philippine Sea plate and backarc spreading along the Izu volcanic arc (e.g., Mazzotti et al., 1999; Nishimura et al., 2018).

The Kanto region was also heavily affected by the 2011 M_w 9.0 Tohoku-oki earthquake, which occurred at the interface between the continental plate and the subducting Pacific plate in the Japan Trench. Although the source region of the 2011 Tohoku-oki earthquake and its aftershocks was limited to northwards of 35.5°N, the Pacific plate subducts beneath the region in the Izu-Ogasawara Trench in the southern region. The overriding plate also changes from the continental plate to the Philippine Sea plate in this area. For simplicity, we hereafter refer to both the combined Japan Trench and Izu-Ogasawara Trench as the Japan Trench. A paleoseismological study has suggested that a M_w 8.3–8.6 tsunami earthquake occurred south of the 2011 Tohoku-oki source region in 1677 (e.g., Yanagisawa et al., 2016). The Kanto and Tokai regions are currently monitored by dense geodetic and seismological instruments.

SSEs in the Kanto and Tokai regions have been detected through long-term observations made by a permanent Global Navigation Satellite System (GNSS) network that was constructed in 1994 and is part of the current nationwide network (GEONET). The M_w ~6.5 SSE detected near the Boso Peninsula in 1996 was one of the earliest observations of an SSE made by continuous GNSS (Figure 1) (Sagiya, 2004). M_w 6.6–6.8 SSEs with durations of ~10 days have repeatedly been observed on the Philippine Sea plate in 2002, 2007, 2011, 2014, and 2018 (e.g., Fukuda, 2018; H. Hirose et al., 2012; Sagiya, 2004). Frequent week-long SSEs with tectonic tremors, which is also called as low frequency tremors occur at depths of 30–40 km west of the Izu Peninsula (e.g., Sekine et al., 2010). They are known as the deep Episodic Tremor and Slip events along the Nankai-Suruga Trough (e.g., Obara, 2011; Obara & Hirose, 2006). Long-term SSEs with durations of several years also occur updip of the tremor zone (e.g., S. Ozawa, 2017; Suito & Ozawa, 2009). On the Pacific

plate, week-long M_w 6.1 SSEs and year-long SSEs have been previously reported by H. Hirose et al. (2001) and Kobayashi and Hirose (2016), respectively. In addition, several studies have noted anomalous seismic swarms that were presumably triggered by SSEs (e.g., Gardonio et al., 2018; Kato et al., 2014; Nishikawa & Ide, 2018). However, a systematic search for SSEs in the Kanto region has not been conducted using GNSS data. In this study, we re-analyze 25 years of GNSS data to detect small SSEs in the Kanto and Tokai regions and discuss the regional characteristics of SSEs and their interplay with regular and slow earthquakes.

2. Data and Methods

2.1. GNSS Data

We used data from a total of 294 GNSS stations located in central Japan (Figure 1). These stations include 288 GNSS Earth Observation Network system (GEONET), four Differential GPS (DGPS), and two International GNSS service (IGS) stations. We estimated the daily coordinates from April 25, 1994 to February 21, 2020 using the GIPSY Ver. 6.4 software package developed by the Jet Propulsion Laboratory (JPL) (https://gipsy-oasis.jpl.nasa.gov). The coordinates were estimated using precise point positioning with ambiguity resolution, then transformed into the IGS14 reference frame (http://acc.igs.org/igs-frames.html) using the Helmert transformation parameters provided by JPL. The number of GNSS stations gradually increased over time; there were 102, 148, 228, and 269 stations by the end of 1994, 1996, 1998, and 2003, respectively.

To preprocess the GNSS coordinates, we first removed any instantaneous steps due to maintenance of the GNSS sites, 14 large intraplate earthquakes with magnitudes between 5.6 and 7.4, the 2008 M_w 6.8 Ibaraki-oki interplate earthquake along the Japan Trench (Nishikawa & Ide, 2018), and five volcanic events in the eastern part of Izu Peninsula. We also removed coseismic and postseismic deformation produced by the 2011 M_w 9.0 Tohoku-oki earthquake and the 2 months of deformation produced by the Miyake-Kozu seismovolcanic activity in the northern Izu Islands during the summer of 2000 (e.g., Nishimura et al., 2001). The deformation associated with the Tohoku-oki earthquake was removed by fitting a simple step and logarithmic decay function to the daily coordinates. For the Miyake-Kozu activity, we calculated the total displacement at the GNSS sites using the dislocation source model of Nishimura et al. (2001) and the temporal evolution, assuming a constant rate from June 26 to August 18, 2000. This was then removed from the daily coordinates. We also removed any anomalous periods exhibiting high scatter or large transients, based on visual inspections and outlier coordinates located beyond three standard deviations. Finally, spatial filtering (Wdowinski et al., 1997) was applied to remove the common mode noises. We hereafter refer to the daily coordinates after preprocessing as cleaned coordinates. Components parallel to the relative plate motions at selected GNSS sites in the cleaned and raw coordinates are shown in Figure 2 and Figure S2, respectively. Distinct downward offsets of up to 30 mm with intervals of 2–6 years were observed at sites 3024 (Figure 2c) and 3041 (Figure 2d) along the Pacific coast of the Boso Peninsula. These offsets are associated with the repeated M_w 6.5–6.8 Boso SSEs (e.g., Fukuda, 2018; Sagiya, 2004). It is difficult to observe signals of less than a few millimeters related to short-term SSEs along the Suruga Trough (e.g., Nishimura et al., 2013; Obara & Hirose, 2006) (Figure 2f). On the other hand, offsets of several millimeters are frequently observed at site 3022, which is the easternmost station in the study area (Figure 2b) and suggests the occurrence of many SSEs along the Japan Trench.

2.2. SSE Detection

We used the method developed by Nishimura et al. (2013) and Nishimura (2014) to detect short-term SSEs, as described here briefly. First, the daily displacements of the north, east, and vertical components were estimated by fitting a linear function to the cleaned coordinates with a step in the middle of a 180 day time window. Daily displacements from July 24, 1994 to November 23, 2019 were estimated by shifting the time window by one day. Second, we focused on the horizontal component parallel to the relative plate motion by rotating the north and east components to detect episodic displacements related to an SSE. The directions of relative plate motion along the Japan Trench, Sagami Trough, and Suruga Trough were assumed to be approximately N80°W, N25°W, and N40°W (Nishimura et al., 2018).

We first sought candidates for dates of possible SSEs by determining the times of relatively well-resolved motions of station subsets that indicated tectonic strain release. The difference in Akaike Information
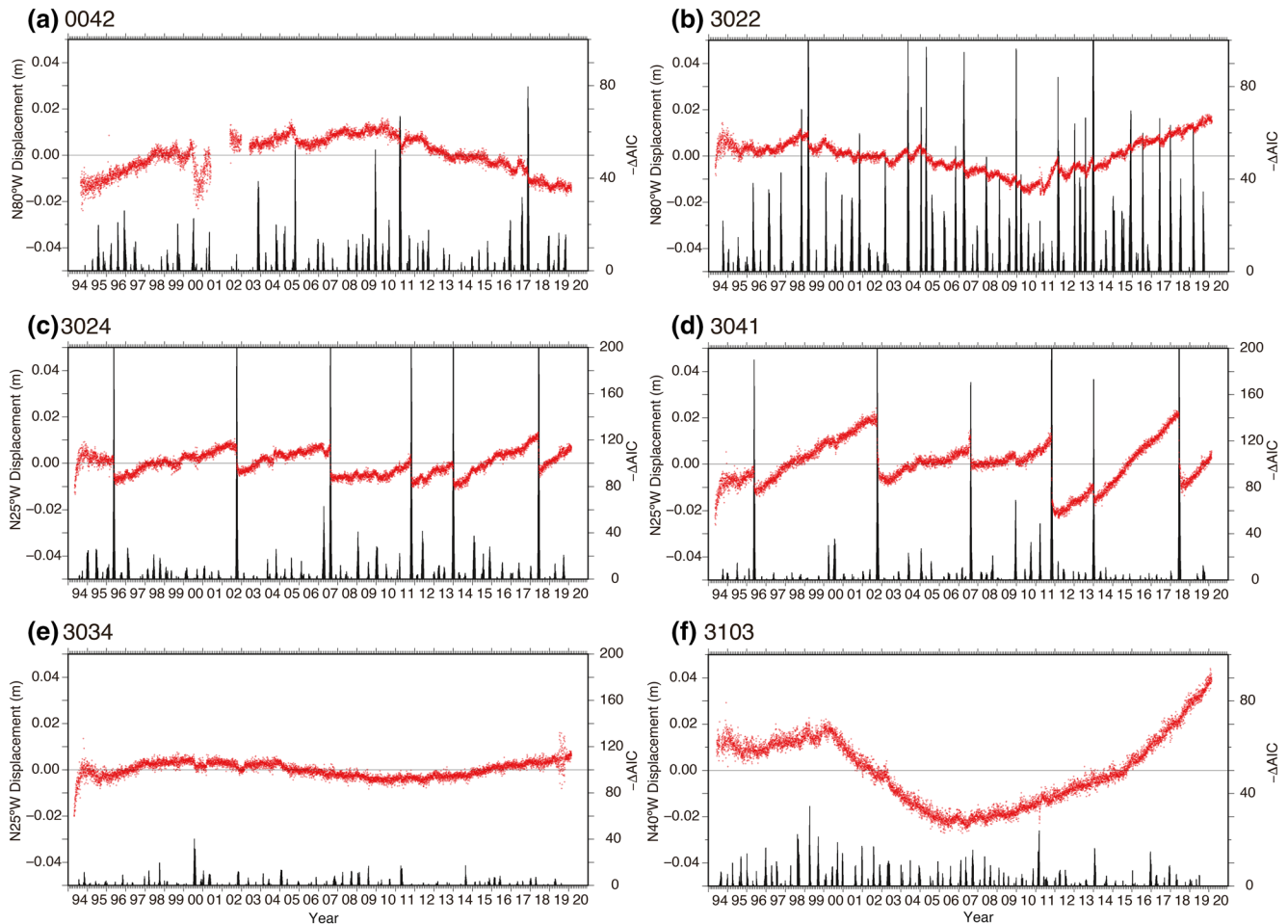
Figure 2. Cleaned coordinates at the selected GNSS stations. See Figure 1 for station locations labeled a-f. A linear trend was removed for plotting. (a) Daily coordinates (red dots) and −ΔAIC (vertical black bars) for the N80°W component at station 0042. (b) Same as (a), but for station 3022. (c) Same as (a), but for the N25°W component at station 3024. (d) Same as (c), but for station 3041. (e) Same as (c), but for station 3034. (f) Same as (a), but for the N40ºW component at station 3103. AIC, Akaike Information Criterion; GNSS, Global Navigation Satellite System.

Criterion (AIC) (Akaike, 1974), ΔAIC, was used to judge which linear functions with and without a step in the middle of a 180 day time window best explain the time series. ΔAIC is calculated by the AIC of the linear and step function minus the linear function. Downward steps in the coordinates clearly corresponded to peaks in negative ΔAIC (Figure 2). A regional average ΔAIC in a 160×50 km^2 rectangular area was calculated for 51 rectangles, with centers indicated by the yellow, orange, and magenta circles in Figure 1 and Figure S1. These points were used to detect SSEs in three separate regions: The Japan Trench, Sagami Trough, and Suruga Trough. The direction of the long side of each rectangular area is parallel to the relative plate motion. Local minima of the average ΔAIC in each region were selected in accordance with both of the following criteria: (1) ΔAIC of less than −3; (2) the lowest ΔAIC in a time range of ±12 days and a distance range of ±0.8 degrees. We found 195, 111, and 77 candidate SSE dates in the three respective regions.

We used the three-dimensional displacement derived from the step amplitude of the time-series fitting on the date of the local minima in ΔAIC at the GNSS sites within a 200 km radius from the point used for the average ΔAIC, then estimated the parameters of a rectangular fault in an elastic half-space (Okada, 1985) using the nonlinear inversion method of Matsu'ura and Hasegawa (1987). We estimated six independent parameters for the rectangular fault (i.e., longitude, latitude, length, width, rake, and slip amount) and the other three parameters (i.e., depth, strike, and dip) were dependent on the horizontal location to approximate the subduction interface (F. Hirose et al., 2008; Nakajima et al., 2009). The estimated parameters depended on the initial parameters in the inversion method used. In order to reduce the dependency of

the initial locations, we began the inversion with 10 sets of initial locations around the point of the average ΔAIC and adopted the parameter set with the smallest residual of the 10 sets. The other initial parameters for the SSEs along the Japan Trench were 40 km, 40 km, 90°, and 10 mm for length, width, rake, and slip, respectively. Parameters along the Sagami Trough and Suruga Trough were the same as those of the Japan Trench, but had a rake of 150°. These parameters are assumed according to previous SSEs in the study region (e.g., H. Hirose et al., 2001; Nishimura et al., 2013; Sagiya, 2004) and do not significantly affect inversion results except for fault sizes for offshore events. The shear modulus is assumed to be 40 GPa.

Once we estimated the fault model (Figure 3), we estimated the duration of the short-term SSEs using the stacked coordinates and the method proposed by Miyaoka and Yokota (2012) as described here briefly. First, we selected coordinates in a 180 day time window whose center is the SSE candidate date for the east and north components of all stations. We removed a linear trend by fitting a linear function to the coordinates for the first and last 60 days of the time window and regarded root mean squares as noise amplitude for the time window. The coordinates were then normalized with the noise amplitude. The amplitude and polarity of the displacement signal in each component were predicted from the estimated fault model. If the fault model predicted a negative polarity (i.e., westward or southward displacement), the coordinate time series were reversed. The normalized coordinate time series were stacked in descending order of each component signal-to-noise ratio (SNR). The key point of this is that the signal amplitude in the stacked time series is the sum of the SNRs for each time series and that its noise amplitude is the square root of the number of stacked time series when noise is not correlated between each component. If the signal in an additional component is small enough to be ignored, the stacking of the additional component increases just the noise amplitude, not the signal amplitude. We therefore stopped stacking when adding additional components would lower the SNR of the stacked time series. The number of stacked components is generally several tens to a few hundred (Figure 4). Stacking GNSS time series has also been used in Frank et al. (2015), Rousset et al. (2017), and Takagi et al. (2019). An advantage of the method of Miyaoka and Yokota (2012) is that it considers not only predicted displacement but also the noise level of each GNSS component.

We regarded the stacked coordinates as a slip time function of an SSE and fit a simple ramp function with a varying duration between 0 and 80 days. The central date of the duration is fixed to the SSE candidate date. Amplitude of the fitted ramp function with a longer duration is generally larger than that of the Heaviside function, which can be regarded as a case of the ramp function with duration of 0 (Figure 4). This suggests that the displacement used for the fault model inversion is generally underestimated because of ignoring duration of the transient deformation, as noted by Nishimura (2014). To correct this underestimation, we estimated the amplitude ratio of the best fitted ramp function and the Heaviside function and multiplied it by the slip estimated in the fault model inversion.

Finally, we categorized the detected events into probable SSEs, possible SSEs, and nonSSEs, based on their slip direction, residual reduction in the fault model inversion, and the SNR of the stacked coordinate time series. Probable SSEs met the following criteria: slip direction within ±20° of the assumed relative plate motion, a variance reduction of more than 100 in the fault model inversion, and a SNR greater than 2.0. The criteria for possible SSEs were a slip direction within ±35º of the assumed relative plate motion and a variance reduction of more than 30 in the fault model inversion. Any events beyond these criteria were designated nonSSEs. Nishimura et al. (2013) empirically decided these criteria by comparing their detected events with SSEs detected with a different data and method (Sekine et al., 2010). The SNR criteria is newly introduced to discard events with poor signals in the time series. In addition, we manually categorized several events as nonSSEs because they were likely attributed to insufficient corrections of large nonSSE events, including the 2011 Tohoku-oki earthquake, the 2004 Off-Kii Peninsula earthquake, the 2008 Ibaraki-oki earthquake, and the 2000 Miyake-Kozu seismovolcanic activity. Dozens of events with overlapping durations were detected in two separate regions as follows: the Sagami Trough and the Japan Trench. We discarded events of lower variance reductions in the fault model inversion for the overlapping events.

3. Results

We detected 64 probable and 112 possible SSEs in the ~25.4 year time series (Figure 5). Parameters and event numbers of the detected SSEs are shown in Figure S3 and listed in Tables S1–S3. The overall distribution of SSEs suggests that SSEs occur at varying depths, but there are several clusters of probable SSEs
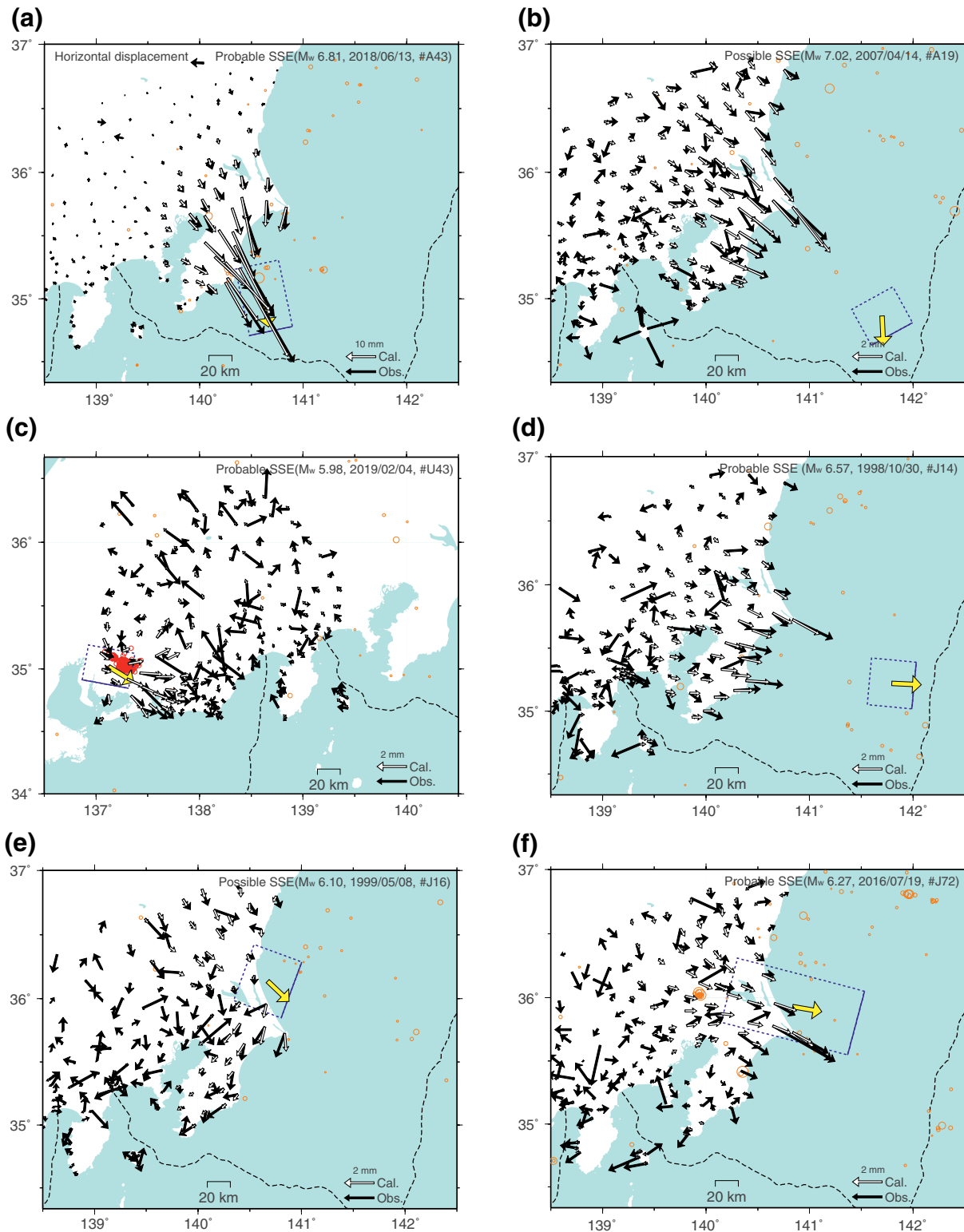
Figure 3. Examples of estimated SSE fault models. Blue dotted rectangles represent the estimated rectangular faults with yellow slip vectors. Solid lines of the rectangular faults represent the shallow edges. Black and white vectors represent observed and calculated displacements. Orange and red circles represent epicenters of regular (M > 2) and LFEs that occurred within 5 days whose central dates are indicated. (a) Probable event on June 13, 2018. (b) Possible event on April 14, 2007. (c) Probable event on February 4, 2019. (d) Probable event on October 30, 1998. (e) Possible event on May 8, 1999. (f) Probable event on July 19, 2016. LFE, low frequency earthquake; SSE, slow slip event.
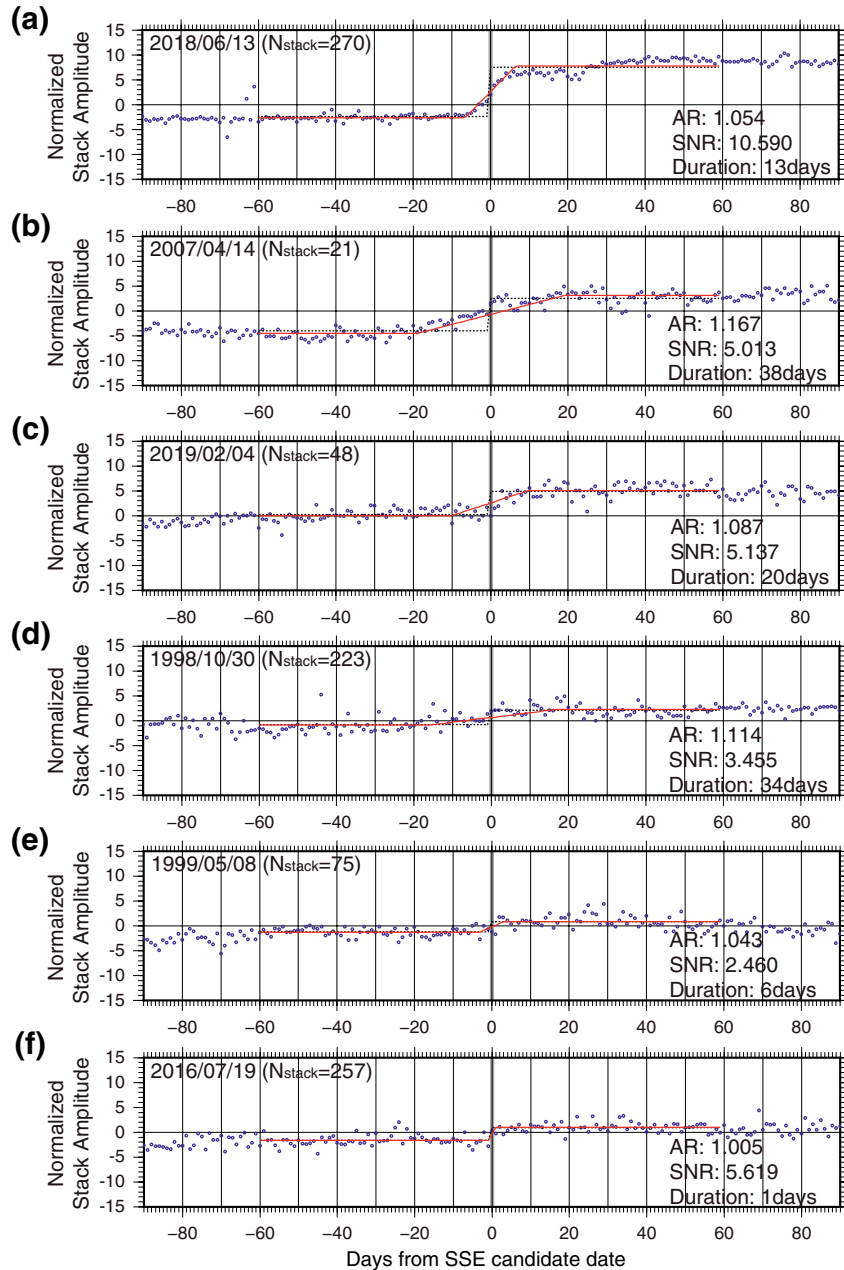
Figure 4. Examples of the stacked coordinate time series. Blue dots are the stacked GNSS time series. Red and black dotted lines are the best fit ramp and Heaviside functions, respectively. The central date of each time window is indicated as the referred SSE candidate date. N_{stack}, AR, SNR, and duration represent the number of stacked components, the amplitude ratio of the best fit ramp and Heaviside functions, the signal-to-noise ratio of the stacked time series, and the duration of the best fit ramp function, respectively. (a–f) correspond to the fault models in Figure 3, respectively. GNSS, Global Navigation Satellite System; SNR, signal-to-noise ratio; SSE, slow slip event.

in limited zones. These zones include a deep (~30–40 km) SSE and tremor zone along the Suruga Trough, two shallow (10–20 km) zones off the Boso Peninsula along the Sagami Trough (Figure 5a), and shallow (10–30 km) and deep (40–80 km) zones along the Japan Trench (Figure 5b). Duration and moment magnitude of the detected SSEs (Figure 6) show a wide variety in these regions and it is notable that $M_w \geq 6.3$ SSEs occur only in an offshore region. The cumulative slip for all probable and possible SSEs (Figure 7) indicates that slip of ≥15 cm is limited within these zones. Although many smaller SSEs were distributed beyond these zones, they had little contributions to accommodating relative plate motion. At the extension
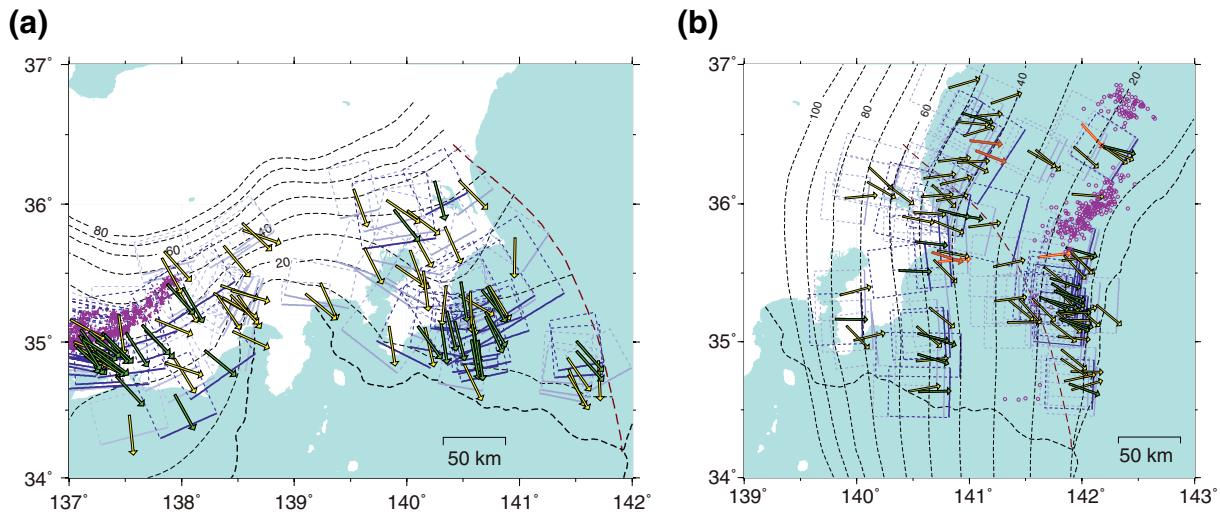
Figure 5. All SSE fault models from July 1994 to November 2019. Thick and thin dotted rectangles indicate the estimated fault models for probable and possible SSEs, respectively. Solid lines of the rectangular faults represent the shallow edges. Green and yellow arrows indicate the slip vectors of probable and possible SSEs, respectively. Red arrows indicate SSEs associated with M ~6 interplate earthquakes. Purple dots indicate epicenters of tectonic tremors (Nishikawa et al., 2019; Obara et al., 2010). (a) All models along the Suruga and Sagami Troughs. (b) All models along the Japan Trench. SSE, slow slip event.

of the deep tremor and slip zone along the Suruga Trough, faint cumulative slip was estimated east of the limit of tremor and vanished near 139°E (Figure 7a), although we cannot rule out misdetection for possible SSEs in this region. Small slip with several interplate earthquakes also occurred around 140°E in the same depth range (30–40 km). An analysis of small repeating earthquakes and seismic attenuation suggests that repeated slow slip occurs in this zone (Nakajima & Uchida, 2018). We discuss the cumulative distributions of regular and slow earthquakes further in Section 4.1.

A magnitude histogram in the three regions indicates that the number of SSEs along the Japan Trench was the largest (Figure 8). Large SSEs with $M_w \geq 6.2$ occurred only along the Sagami Trough and Japan Trench. The moment magnitudes of the most frequent SSEs were 6.2 and 5.9 along the Japan Trench and Suruga Trough, respectively. The numbers of detected SSEs below and above the peaks were lower, which suggests the limited detection capability of our GNSS network and a lower frequency for larger SSEs, respectively. The larger peak magnitudes along the Japan Trench indicate a lower detection capability for offshore SSEs
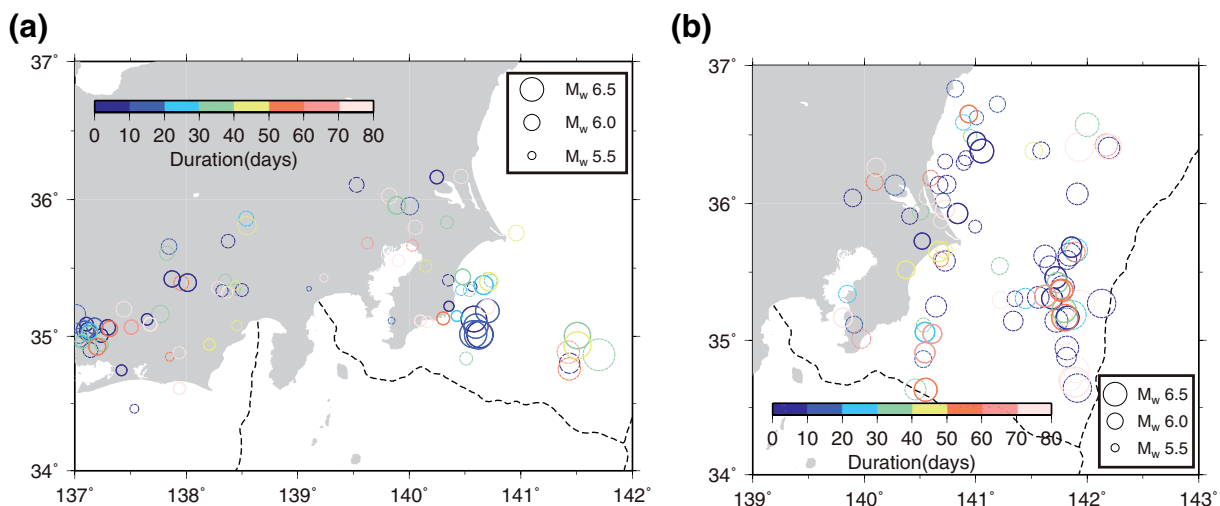

Figure 6. Duration for all detected SSEs. Circles with solid and broken lines indicate probable and possible SSEs, respectively. (a) Duration of detected SSEs along the Suruga and Sagami Troughs (b) Same as (a), but along the Japan Trench. SSE, slow slip event.
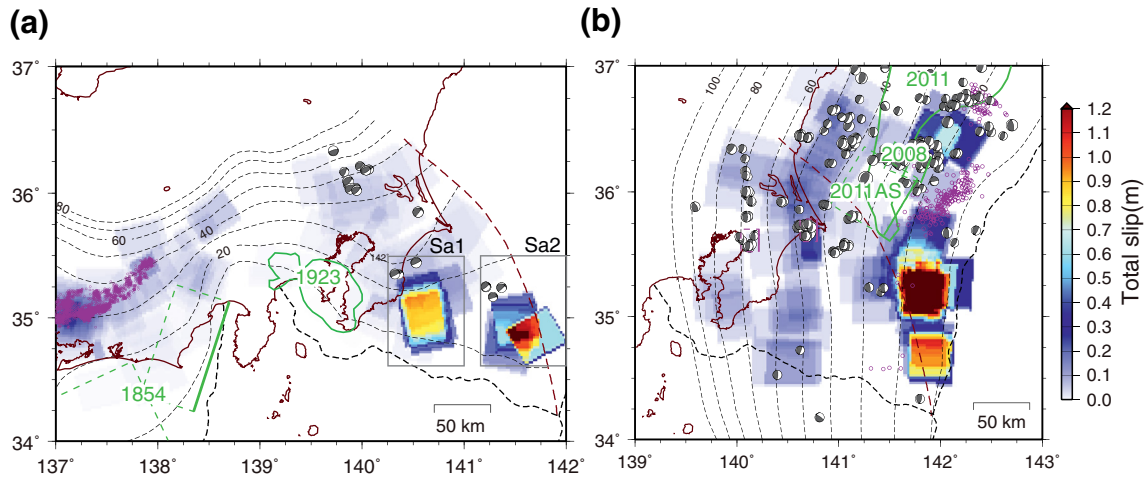
Figure 7. Cumulative slip distributions of SSEs from July 1994 to November 2019. Green areas and rectangles indicate the source areas of past megathrust earthquakes with their occurrence years. Purple dots and circles indicate epicenters of tectonic tremors (Nishikawa et al., 2019; Obara et al., 2010). Focal mechanisms of $M_w \geq 4.8$ interplate earthquakes from 1997 to 2019 determined by NIED are also plotted. (a) Slip along the Suruga and Sagami Troughs. Gray rectangles Sa1 and Sa2 indicate the regions used for plotting moment evolutions (Figure 10). (b) Slip along the Japan Trench. NIED, National Research Institute for Earth Science and Disaster Prevention; SSE, slow slip event.

using land-based GNSS data. The histogram along the Sagami Trough exhibits a scattered distribution above the peak magnitude (M_w 5.7), with a second peak at approximately M_w 6.7. This second peak magnitude corresponds to the Boso SSEs that occurred in 1996, 2002, 2007, 2011, 2014, and 2018 (e.g., Fukuda, 2018; H. Hirose et al., 2012; Sagiya, 2004). Considering the detectability of SSEs in the region around the Boso SSEs, the Boso SSEs are characteristic events that can be distinguished from the other smaller SSEs, forming an exponential or power law distribution. Of the detected SSEs, 110 of the 176 had a duration of more than 14 days, which means that the detection method of Nishimura et al. (2013), which was originally developed to detect short-term SSEs, can be applied to intermediate-term SSEs with durations of less than a few months. No previous studies have reported the largest M_w 7.0 SSE (event #A19), detected near the triple junction along the Sagami Trough (Figure 3b). The stacked GNSS time series of this event clearly shows a month of transient deformation (Figure 4b). Observing such a distinctive event highlights the importance of conducting a systematic search for SSEs.

The estimated SSE duration determined by stacking time series data (Figure 6) is fairly reasonable for the high SNR events. The durations of the Boso SSEs in 1996, 2002, 2007, 2011, 2014, and 2018 (event #s A02, A13, A21, A30, A34, and A43) were estimated to be 11, 10, 7, 11, 13, and 13 days, respectively. Their SNR ranged between 6.3 and 21.7. The duration is concordant with periods of high moment release rates
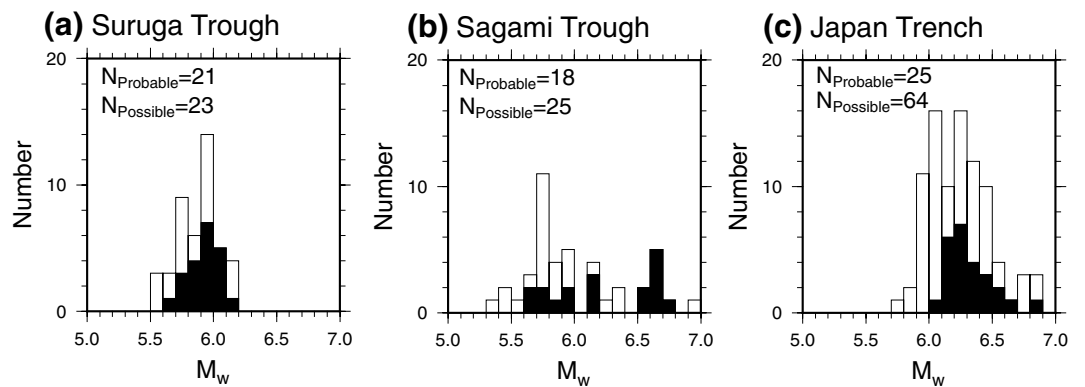

Figure 8. Moment magnitude histograms of estimated SSEs in three regions. Solid and open bars indicate the number of probable and possible SSEs, respectively. (a) Along the Suruga Trough. (b) Along the Sagami Trough. (c) Along the Japan Trench. SSE, slow slip event.
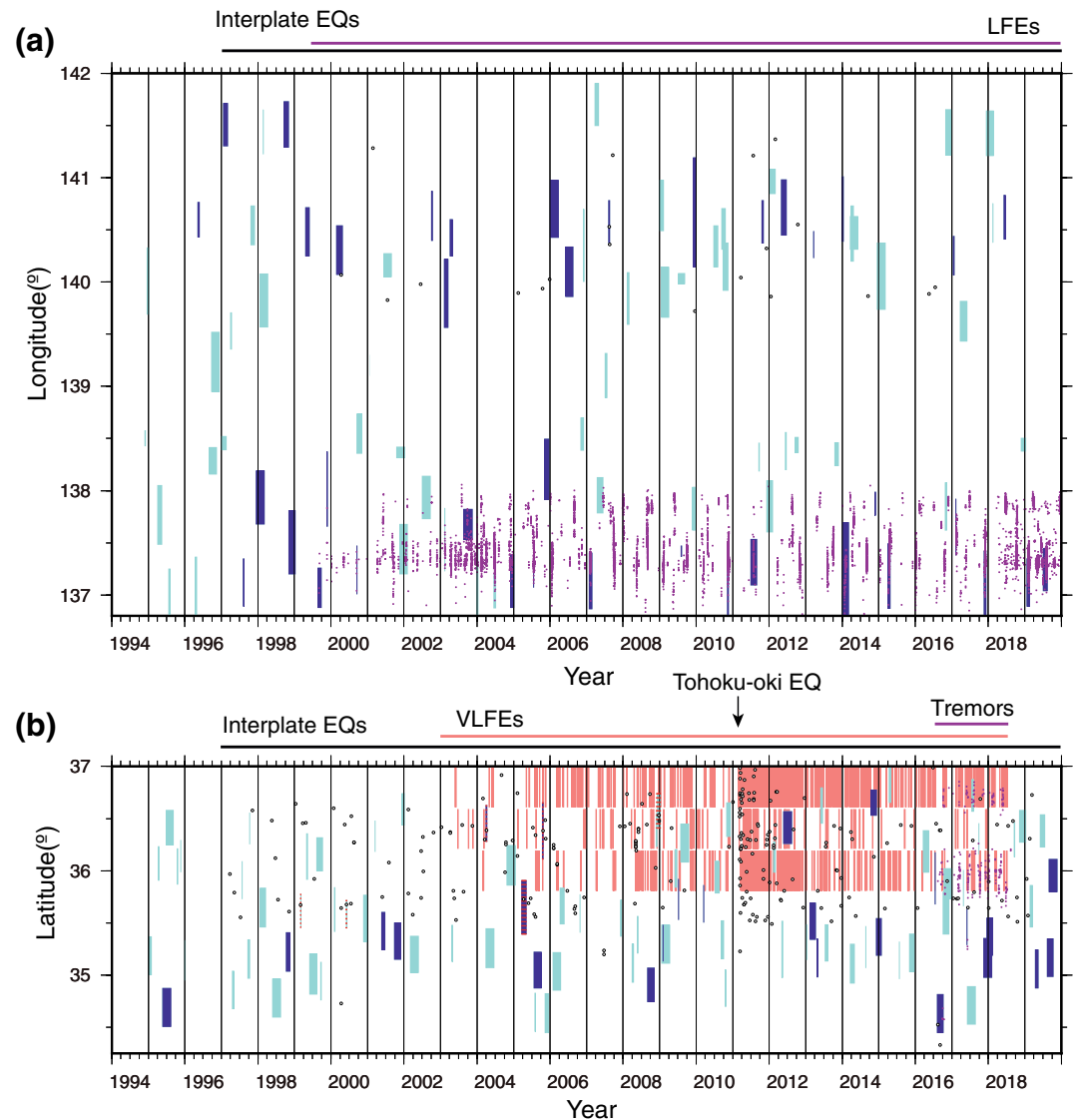
Figure 9. Space-time plot of detected SSEs. Blue and light-blue rectangles indicate the spatial extents and durations of probable and possible SSEs, respectively. Open circles indicate the centroids of the $M_w \geq 4.8$ interplate earthquakes whose focal mechanisms were determined by NIED. (a) SSEs along the Sagami and the Suruga Troughs. The vertical axis indicates the longitudinal extent. Purple dots indicate LFE epicenters determined by JMA. (b) SSEs along the Japan Trench. The vertical axis indicates the latitudinal extent. Thin red bars indicate VLFEs (Baba et al., 2020). Rectangles with red horizontal stripes indicate SSEs related to $M_w \geq 5.8$ interplate earthquakes. Purple dots indicate tremor epicenters determined by Nishikawa et al. (2019). Note that each catalog covers a limited temporal extent: interplate earthquakes (January 1997–), VLFEs (January 2003–July 2018), LFEs (July 1999–), and tectonic tremors (August 2016–August 2018), as shown by horizontal bars over each subfigure. NIED, National Research Institute for Earth Science and Disaster Prevention; SSE, slow slip event; VLFE, very low frequency earthquake.

estimated by previous studies (e.g., Fukuda, 2018). However, the estimated duration of the events in the SSE zone along the Suruga Trough ranged from 1 to 80 days (Figure 6a), which is generally longer than those (i.e., 3–7 days) of the short-term SSEs determined from tiltmeter data (Sekine et al., 2010). Durations longer than the corresponding tremor clusters of the detected SSEs can be observed in the space-time plot of SSEs and regular and slow earthquakes shown in Figure 9a. There are several reasons for this apparent discrepancy. First, the estimated durations have large uncertainties for low SNR events, which is attributed to the low SNR of the data, as well as to our simplified assumption in estimating the durations. We fixed the middle date of each SSE episode based on the ΔAIC minimum and only estimated the duration around

the middle date to obtain a stable estimation. In the case of the highest SNR (5.1) events along the Suruga Trough (event #U43, Figure 3c), the stacked time series (Figure 4c) suggests that significant displacement continued after the date of the ΔAIC minimum. This may occur because the GNSS stations used were not the same as those used for averaging the ΔAIC and stacking the time series. When the middle date of the SSE deviates from the middle of the transient displacement in the stacked time series, the duration is likely overestimated. Second, the detected SSEs have longer durations than previously observed short-term SSEs accompanying tremors. The short-term and long-term SSEs along the Suruga Trough overlap significantly (Suito & Ozawa, 2009). An event detected on October 4, 2003 with duration of ≥ 80 days (event #U17) may have been an accelerated slip phase during the long-term Tokai SSE. In addition, our detection method simplifies multiple intermittent slip events into a single event. Indeed, analyses using strain and tilt data (e.g., GSJ & NIED, 2014) separate the detected SSEs (e.g., event #s U36, U38, and U44) into a few intermittent episodes. Although these factors may bias the estimated durations toward longer periods of time, some stacked time series with high SNRs demonstrated the existence of SSEs with a duration of more than several weeks, including event #A19 (Figures 3b and 4b).

Six SSEs (event #s J15, J21, J29, J32, J35, and J45) were related to $M_w \geq 5.8$ interplate earthquakes along the Japan Trench (denoted by striped symbols in Figure 9b). Notably, the estimated moments of these SSEs were ~2–8 times that of the related earthquake, except for event #J45, which had a similar moment. We separated event #J45 because its stacked time series shows transient movement. All of the related earthquakes occurred 0–4 days before the date of the detected SSE, which can be regarded as coseismic slip and afterslip. Hawthorne et al. (2016) shows that postseismic moments for many M > 6 earthquakes typically display only a few tens of percent of the coseismic ones in the world. It is a regional characteristic that large afterslip following interplate earthquakes is often observed along the Japan Trench (e.g., Kawasaki et al., 2001; Suito et al., 2011)

4. Discussion

4.1. Characteristics of Slow Slip Distribution with Regular Earthquakes and Low Frequency Tremors

Most SSEs observed globally have complementary locations with the asperities of huge megathrust earthquakes or interseismic locked patches (e.g., Dixon et al., 2014; Schwartz & Rokosky, 2007). Our results also support this relationship. Tectonic tremors, consisting of successive low frequency earthquakes (LFEs), are often accompanied by SSEs worldwide (e.g., Frank, 2016; Fujita et al., 2019; Schwartz & Rokosky, 2007). Very low frequency earthquakes (VLFEs) are often collocated with SSEs. Tectonic tremors, LFEs, and VLFEs presumably rupture small seismic patches on the plate interface and are interpreted to be triggered by surrounding slow slip. Therefore, they are sometimes regarded as a proxy for SSEs. (Baba et al., 2020; Y. Ito et al., 2007; Schwartz & Rokosky, 2007; Wech et al., 2009). In the study area, deep tremors occur at depths of 30–40 km along the Suruga Trough (e.g., Obara et al., 2010), whereas shallow tremors occur at depths of 10–20 km along the Japan Trench (Nishikawa et al., 2019). No tremors have been reported along the Sagami Trough. VLFEs are observed around the shallow tremor region along the Japan Trench (Baba et al., 2020). Here we compare the distributions of detected SSEs with low-frequency and regular earthquakes in each region (i.e., the Suruga Trough, Sagami Trough, and Japan Trench) and discuss their characteristics in detail.

Along the Suruga Trough, most of the probable SSEs coincide with tremors, as noted by previous studies (e.g., Sekine et al., 2010), although tremor episodes occur much more frequently than the SSEs (Figure 9a). This suggests the limited detection capability of small SSEs when using GNSS data. The studies using strain and tilt data detected smaller SSEs associated with tremors in these regions (GSJ and NIED, 2014; Sekine et al., 2010). Although our previous study (Nishimura et al., 2013) detected ≥10 probable SSEs updip of the tremor zone, this study detected only two probable SSEs. Most of the SSEs detected by Nishimura et al. (2013) are probably false events due to artificial errors produced by common-mode noise reduction for a wide region. Although we cannot completely rule out the false detection of two probable SSEs (event #s U08 and U22) in this study, they may be real medium-term SSEs updip of the short-term SSE zone because long-term SSEs occurred in the same depth range in 2001–2005 and 2013–2015 (S. Ozawa, 2017). Few SSEs (Figure 5a) and a small cumulative slow slip (Figure 7a) were observed in the source areas of the 1854 M_w 8.0 Ansei Tokai earthquake.

Along the Sagami Trough, there are two distinct regions of high cumulative slip at 10–20 km. One is the region of the well-known Boso SSEs, denoted as Sa1 in Figure 7a, and the other is further offshore near the eastern edge of the subducting Philippine Sea plate, denoted as Sa2 in Figure 7a. Cumulative slip in these regions is comparable to relative plate motion for the time period analyzed (∼76 cm for 25.4 years). M_w ∼5 interplate earthquakes occur at the downdip edge of both high slip regions, as well as deep moderate slip at ∼40 km. The swarm-type earthquake activities in the Boso SSE region are explained by stress triggering due to SSEs (Fukuda, 2018; Gardonio et al., 2018; H. Hirose et al., 2012). The spatial relationship between these SSE regions also suggests that stress triggering occurs at the edges of SSE regions (Figure 7a), although we do not observe clear temporal correlations between SSEs and $M_w \geq 4.8$ interplate earthquakes in the last 23 years (Figure 9a). Shallow SSE regions are in the same depth range as the 1923 M_w 7.9 Kanto earthquake, but are complementary along the Sagami Trough (Figure 7a). There are two significant gaps in high cumulative slow slip and earthquake asperity at 140°E and 141°E. The former may be filled by coseismic slip from the aftershocks of the 1923 earthquake and past Kanto earthquakes. No slip events in the latter have been observed. Because land GNSS data do not have sufficient resolution to observe this gap (e.g., Nishimura et al., 2018), offshore GNSS-Acoustic measurements are necessary to evaluate the potential of a large earthquake. Variations of large fast earthquakes and slow slip in a depth range of ≤20 km along the Sagami Trough cannot be explained by a long wavelength change in thermal condition (Wada & He, 2017). A. Ito, Yamamoto, et al. (2017) observed pronounced low velocity anomalies in both P- and S- waves, with low V_p/V_s ratios (1.5–1.6) in the offshore SSE region of the overriding plate and interpreted that this indicates both the presence of quartzite and water. A shallowing of the plate interface is also inferred by A. Ito, Sugioka, et al. (2017). These heterogeneities in and around the megathrust fault and the irregular geometry of the megathrust fault itself may control the conditions required for fast and slow slip.

Along the Japan Trench, cumulative slow slip has a bi-modal depth distribution at depths of ∼10–30 km and ∼40–80 km (Figure 7b). This spatial pattern is very similar to that of average slip rates estimated from small repeating earthquakes from 2001 to 2019 (Igarashi, 2020). Many M_w ∼5 interplate earthquakes also occur in and around slow slip areas, which can be interpreted as scattered seismic patches on a quasicreeping fault along the Japan Trench (Igarashi et al., 2003). Several SSEs can be interpreted as co- and postseismic slip following M_w ∼6 interplate earthquakes as described above and shown in Figure 7b. At depths of ∼40–80 km, two long-term M_w 6.4 and M_w 6.5 SSEs in 2000 and 2005 were reported by Kobayashi and Hirose (2016). Fast and slow slip with a wide range of durations are co-located in the same depth range. Slip at an intermediate depth of ∼30–40 km is mainly accommodated by coseismic slip of large earthquakes, including the 2011 Tohoku-oki earthquake, its largest aftershock, and the 2008 M_w 6.8 Ibaraki-oki earthquake. Relatively low interplate seismicity and slow slip are observed in this depth range south of 35.5°N (Figure 7b). This region is a candidate source region for a large tsunami earthquake in 1677 (e.g., Yanagisawa et al., 2016) and may have the potential to produce future large earthquakes.

It is notable that the detected shallow SSEs and tremors (Nishikawa et al., 2019) occur in the same depth range, but have complementary distributions along the Japan Trench (Figures 5b and 6b). Only two SSEs have a close proximity in time and space with the tremors. One is a shallow SSE that occurred on June 3, 2017 (event #J77), with a few tremors at the southern edge of the SSE fault, as noted by Nishikawa et al. (2019). This was followed by more intense tremor activity north of the SSE a week after the SSE onset. The other is an SSE near the coast that occurred on July 17, 2017 (event #J79). Tremors were activated 50 km offshore of the estimated SSE fault at the end of the estimated duration (19 days). We speculate a possible cause of the apparent complementary distribution as follows. Common tremor characteristics of episodicity and along-strike migration in the Nankai Trough and on the Cascadia margin suggest that tremors along the Japan Trench are triggered by slow slip (e.g., Ando et al., 2010). However, the slow slip in the tremor regions along the Japan Trench may not cause observable surface displacements at land GNSS stations. Indeed, major tremor clusters around 36°N activate several times a year (Nishikawa et al., 2019). Even if all of the relative plate motion (i.e., ∼8 cm/yr) is accommodated by SSEs in the tremor region, the average slip of each SSE associated with a major tremor episode will be less than 2 cm, which is less than half of that of the nearby smallest SSEs detected in this study. Because 4–6 cm/yr of interplate slip rates in the tremor region can be estimated from small repeating earthquakes (Igarashi, 2020), SSEs in the tremor region have much smaller slips and are probably too small to be detected from land GNSS data. On the other hand, it is still unclear why tremors rarely occur in the shallow SSE regions. No tremors with significant slow slip have
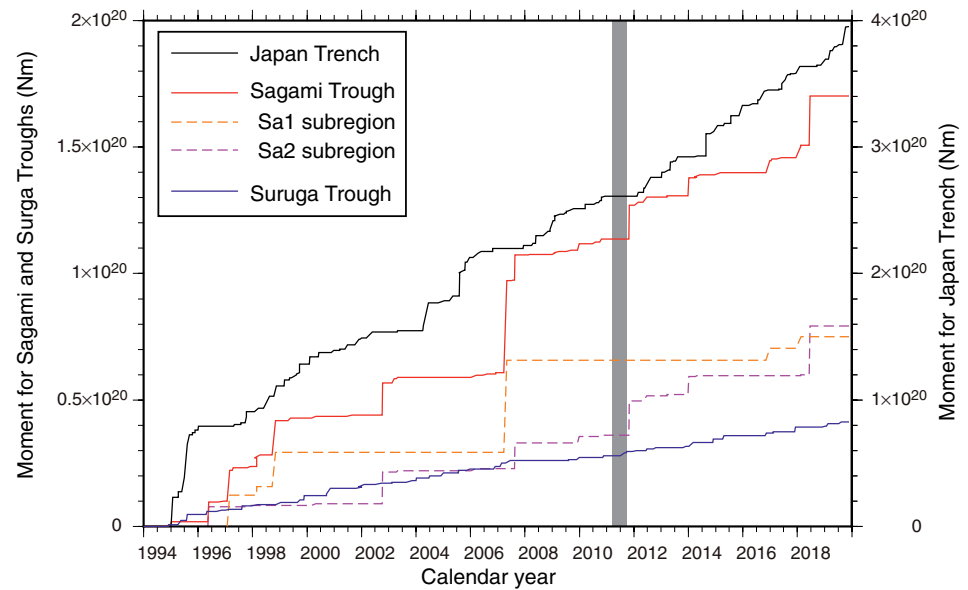
Figure 10. Moment release evolution of the detected SSEs. Note that the moment vertical scale is different for the Suruga and Sagami Troughs and the Japan Trench. Shading indicates the lower detection ability due to large postseismic displacements for 6 months following the Tohoku-oki earthquake. SSE, slow slip event.

been reported in deep slow slip zones like the tremor gap at Ise Bay along the Nankai Trough (Nishimura et al., 2013). Nakajima and Hasegawa (2016) found that LFEs do not occur in a region where P- and S-wave velocities are lower than approximately −4% along the Nankai-Suruga-Sagami Trough, including the Ise Bay gap. A low P-wave anomaly in the overlying plate is also observed in the shallow SSE regions along the Japan Trench (Liu & Zhao, 2018). This may support the hypothesis that low LFE activity forming a tremor gap can be attributed to the relatively high strength of the megathrust fault under well-drained conditions due to the high permeability of the overlying plate (Nakajima & Hasegawa, 2016).

We also calculated approximate stress drop ($\Delta\sigma$) by using $\Delta\sigma \approx \mu D / L$, where μ is the shear modulus, D is the slip and L is the square root of the slip area (Figure S4). Stress drop ranges between ~1 and 600 kPa and shows regional variations. Most SSEs with stress drop of ≥100 kPa occur in an offshore region. The Boso SSEs with large stress drop are surrounded by SSEs with smaller stress drop, which may reflect the spatial variation on fault strength of the plate interface. However, we need a further clarification of uncertainties of the calculated stress drop to discuss regional characteristics, in particular along the Japan Trench. The calculated stress drop for offshore events is highly dependent on initial fault parameters of the fault size because land GNSS data constrain only the product of slip and fault size (i.e., potency) not each of them.

4.2. Temporal Evolution of SSE Moment over 25 Years

Moment evolution released by SSEs for 25 years differs in the three regions (Figure 10). Large steps associated with the ~10 largest SSEs dominate the total moment increase along the Sagami Trough, whereas small steps form a gradual moment increase along the Suruga Trough. Moment evolution along the Japan Trench is intermediate. The total moment along the Japan Trench is more than twice that of the other regions. There are no clear long-term changes in moment rate, even during the 2011 M_w 9.0 Tohoku-oki earthquake, in any of the three regions. This may be a contrast to the observation that the mainshock and postseismic deformation imposed large changes in stress and stress rates on the analyzed regions (e.g., S. Ozawa et al., 2012; Toda et al., 2011) and stimulated VLFEs (Baba et al., 2020) and regular earthquakes (Figure 9b). We speculate that the reason for no apparent change during the Tohoku-oki earthquake is as follows. Our detection method is not sensitive to continuous postseismic slip. We removed a logarithmic postseismic displacement during preprocessing and our method determined slip acceleration from the average slip in the time window (i.e., 180 days). In addition, high scattering of preprocessed GNSS data more than 3 months after the Tohoku-oki earthquake must have degraded the detectability of SSEs in our analysis (Figure 9b). The

scattering can be attributed to the oversimplification of the fitted logarithmic functions used for postseismic deformation, insufficient correction for the two M ∼7 intraplate earthquakes that occurred on April 2011, and numerous unmodeled M ∼6 earthquakes in the regions. In addition, slip behavior on an SSE patch may change after a large stress perturbation, as long-term transient afterslip occurred for 8 years on an SSE patch in southwest Japan (Yarai & Ozawa, 2013). Along the Suruga Trough, the coseismic stress change due to the Tohoku-oki earthquake was estimated on the order of kPa (Toda et al., 2011) and is likely not large enough to modulate the SSE activity in the region.

4.3. SSEs Corresponding to Earthquake Swarms

Our detected SSEs do not correspond to earthquake swarms observed by previous studies (Gardonio et al., 2018; Kato et al., 2014; Okutani & Ide, 2011), except for three Ibaraki-oki swarms along the Japan Trench in January 1995, March 2004, and March 2006 (Nishikawa & Ide, 2018). However, our estimated fault models (event #s J01, J29, and J37) are located in the Ibaraki-oki swarm region (36.2ºN, 142.0ºE). This implies that our detected SSEs may indicate a slip concentration part of the accelerated slip over a much wider region of the plate interface, because slip of our fault model exceeding 3 cm is larger than the ∼1 cm of slip estimated from small repeating earthquakes in the Ibaraki-oki swarm region. The other swarms were too small for geodetic methods to detect significant displacements or are still hidden in the large postseismic displacement that occurred after the 2011 Tohoku-oki earthquake (Kato et al., 2014).

Synchronization of our detected SSEs with not only regular earthquakes, but also other slow earthquakes including VLFEs and tectonic tremors, is limited except for the short-term SSEs along the Suruga Trough and the repeated Boso SSEs (Figure 5). Distributions of small patches that host VLFEs, tremors, and regular earthquakes in and around a slow slip region (Ando et al., 2010; Igarashi et al., 2003; Y. Ito et al., 2007) can cause apparent triggering differences for these seismic events. Gardonio et al. (2018) related a transient displacement to an earthquake swarm along the Sagami Trough in March 2018, but a displacement pattern at a number of GNSS stations clearly suggests that it is related to an SSE along the Japan Trench (event #J51), not along the Sagami Trough. It is clear that increasing the amount of data is necessary to resolve such discrepancies.

4.4. Future Prospects for SSE Detection

Although our method succeeded in detecting small transient displacements, it is difficult to estimate where and what type of slow slip will occur in an offshore region only from land GNSS displacements. Although we assumed that all SSEs occurred on the subducting plate interface and used a slip angle relative to the plate motion as a criterion to distinguish the SSEs, the detected SSEs may include intraplate events and simultaneous SSEs on both the Pacific and Philippine Sea plates. Significant coseismic displacements were observed for several intraplate earthquakes at GNSS stations after the 2011 Tohoku-oki earthquake. Some of these were reproduced by slip at the plate interface. We corrected the displacements of these events in the preprocessing of the GNSS data, but some uncorrected displacements may have affected our results. We also found that offshore slip on both the Philippine Sea plate and the Pacific plate around 35°N, 142°E caused similar eastward displacements at land GNSS stations. These slip events may be confused in our SSE catalog.

Many individual SSEs can cause small surface deformations below the noise levels of geodetic measurements. Although many methods including this study have been proposed to detect small SSEs (e.g., Haines et al., 2019; Rousset et al., 2017), the current geodetic methods have limited resolving power for individual SSEs. Recent successes in detecting SSE related displacements by stacking GNSS data based on seismological information demonstrates a way to overcome the limitation in both temporal and spatial resolution (e.g., Frank, 2016; Frank et al., 2015; Fujita et al., 2019; Bartlow, 2020). The limited synchronization between SSE and earthquakes in central Japan suggests a complementary relationship between SSEs and seismological events. Combining various types of geodetic and seismological data can help to clarify the mechanisms and slip budgets of fast and slow slip on the plate interface.

We also noticed a limitation in uniform slip along a single rectangular fault in our method. Although a large source region was estimated for an SSE along the Sagami Trough on December 18, 2009 (event #A26), its
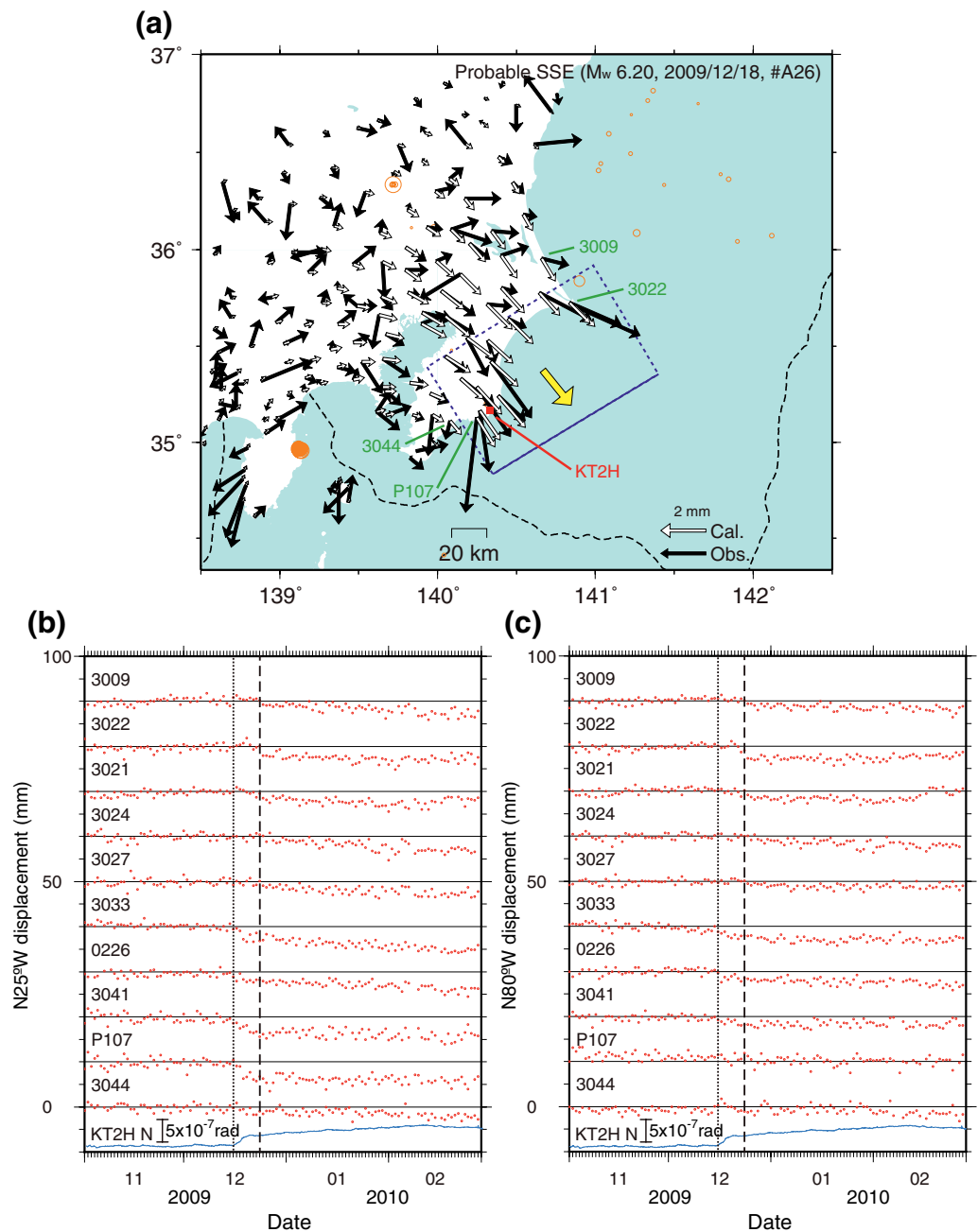
Figure 11. An SSE that occurred around December 18, 2009. It is likely that slow slip successively occurred along both the Sagami Trough and the Japan Trench (See text). (a) An estimated single rectangular fault model (dotted rectangle) along the Sagami Trough. The solid line of the rectangular fault and the yellow arrow indicate the shallow edge and the slip vector, respectively. The green characters indicate the GNSS stations whose time series are plotted in (b) and (c). KT2H is a borehole tiltmeter station. (b) GNSS time series in the N25°W direction, parallel to interplate slip along the Sagami Trough. The time series are arranged from the northeastern stations to the southwest stations along the coast. The bottom blue line shows the northward component of tilt at KT2H (NIED, 2010a). (c) GNSS time series in the N80°W direction, parallel to interplate slip along the Japan Trench. GNSS, Global Navigation Satellite System; NIED, National Research Institute for Earth Science and Disaster Prevention; SSE, slow slip event.

fault model (Figure 11a) is probably biased because the event may have consisted of two successive SSEs along the Sagami Trough and the Japan Trench. The GNSS time series on the Boso Peninsula exhibits a transient displacement in the middle of December (Figures 11b and 11c). Transient displacements toward

the south or south-southeast began at southwestern stations (e.g., P107) around December 16 and concluded within a week. However, transient displacements toward the east or east-southeast were delayed at northeastern stations (e.g., 3022) and began around December 24. This transient deformation was recorded only by a borehole tiltmeter (KT2H) (Figures 11a–11c) and was modeled by a 10×10 km^2 rectangular fault located near the KT2H station (NIED, 2010b). It is unlikely that the source area extended to the northeast, as estimated in this study, because no significant tilt changes were observed by the other tiltmeters. A different direction and temporal delay of the transient displacement at the northeastern stations suggests that another event similar to event #J14 (Figure 4d) occurred along the Japan Trench after the event near the KT2H station. It is inevitable that the model be simplified because most of the SSEs detected in this study produced small displacements of a few millimeters. To avoid oversimplification, it is important to increase the number of observation points and combine multiple geodetic techniques, including GNSS, tilt, strain, gravity, and offshore pressure gauges. Offshore geodetic networks are currently deployed along the subduction zones, including Japan, New Zealand, and Cascadia, and will help with further clarification of offshore SSEs.

5. Conclusions

We developed a detection method for SSEs (Nishimura, 2014; Nishimura et al., 2013) to estimate the duration of an SSE, which we then applied to GNSS data from the Kanto and Tokai regions of central Japan from 1994 to 2020. We found 76 probable and 103 possible SSEs in a ~25.4 year time period. Most of these events had not been previously identified, including offshore shallow (~10 km) and inland deep (~40 km) SSEs along the Sagami Trough, as well as many shallow SSEs along the Japan Trench. Although our detection method focuses on short duration events, the detected SSEs had a wide variety of moment magnitudes (5.3–7.0) and durations (0–80 days). The average magnitudes of SSEs without LFEs and tectonic tremors along the Japan Trench and Sagami Trough were larger than those with tremors along the Suruga Trough. Cumulative slip of the SSEs along the Japan Trench exhibited a bi-modal depth distribution at 10–30 and 40–80 km, which are updip and downdip of the source regions of large megathrust earthquakes. Tectonic tremors also occurred in the shallow depth range, but rarely overlapped with detected SSEs.

Our results show limited correlations between SSEs and other regular and slow earthquakes, which suggests that variations in fault slip behavior are controlled by many factors, including temperature, pressure, fault geometry, porefluids, and the properties of the overlying plate. We found no clear changes to moment evolution of SSEs for 25 years in spite of the 2011 M$_w$ 9.0 Tohoku-oki earthquake, suggesting stress and/or stress rates are not the only factors controlling SSE genesis. This study supports complementary distribution between SSEs and large megathrust earthquakes, which can contribute to evaluation of earthquake potential in the subduction zone.

Data Availability Statement

GNSS RINEX data were provided by the Geospatial Information Authority of Japan, Japan Coast Guard, and the International GNSS service, and are available at http://datahouse1.gsi.go.jp/terras/terras_english.html, https://www1.kaiho.mlit.go.jp/KOHO/dataservice/htdoc1.html, and https://cddis.nasa.gov/archive/gnss/data/daily/, respectively. Earthquake catalogs, including low-frequency earthquakes and focal mechanism by the Japan Meteorological Agency and National Research Institute for Earth Science and Disaster Resilience, are available at https://www.data.jma.go.jp/svd/eqev/data/bulletin/hypo.html and https://www.fnet.bosai.go.jp/fnet/event/joho.php?LANG=en, respectively. Catalogs of low-frequency tremors and very low-frequency earthquakes along the Japan Trench are from summplements in Nishikawa et al. (2019) and Baba et al. (2020), respectively. The figures were prepared using the Generic Mapping Tools (Wessel et al., 2013), which are available at https://www.generic-mapping-tools.org.

References

Akaike, H. (1974). A new look at the statistical model identification. *IEEE Transactions on Automatic Control*, *19*, 716–723. https://doi.org/10.1109/TAC.1974.1100705

Ando, R., Nakata, R., & Hori, T. (2010). A slip pulse model with fault heterogeneity for low-frequency earthquakes and tremor along plate interfaces. *Geophysical Research Letters*, *37*(10), L10310. https://doi.org/10.1029/2010gl043056

Baba, S., Takeo, A., Obara, K., Matsuzawa, T., & Maeda, T. (2020). Comprehensive detection of very low frequency earthquakes off the Hokkaido and Tohoku Pacific Coasts, Northeastern Japan. *Journal of Geophysical Research: Solid Earth*, *125*(1), e2019JB017988. https://doi.org/10.1029/2019jb017988

Bartlow, N. M. (2020). A long-term view of episodic tremor and slip in Cascadia. *Geophysical Research Letters*, *47*, e2019GL085303. https://doi.org/10.1029/2019GL085303

Dixon, T. H., Jiang, Y., Malservisi, R., McCaffrey, R., Voss, N., Protti, M., & Gonzalez, V. (2014). Earthquake and tsunami forecasts: relation of slow slip events to subsequent earthquake rupture. *Proceedings of the National Academy of Sciences of the U S A*, *111*(48), 17039–17044. https://doi.org/10.1073/pnas.1412299111

Frank, W. B. (2016). Slow slip hidden in the noise: The intermittence of tectonic release. *Geophysical Research Letters*, *43*(19), 10125–10133. https://10.1002/2016gl069537

Frank, W. B., Radiguet, M., Rousset, B., Shapiro, N. M., Husker, A. L., Kostoglodov, V., et al. (2015). Uncovering the geodetic signature of silent slip through repeating earthquakes. *Geophysical Research Letters*, *42*, (8), 2774–2779. https://doi.org/10.1002/2015gl063685

Fujita, M., Nishimura, T., & Miyazaki, S. (2019). Detection of small crustal deformation caused by slow slip events in southwest Japan using GNSS and tremor data. *Earth, Planets and Space*, *71*, 96. https://10.1186/s40623-019-1075-x

Fukuda, J. (2018). Variability of the space-time evolution of slow slip events off the Boso Peninsula, Central Japan, From 1996 to 2014. *Journal of Geophysical Research: Solid Earth*, *123*(1), 732–760. https://doi.org/10.1002/2017jb014709

Gardonio, B., Marsan, D., Socquet, A., Bouchon, M., Jara, J., Sun, Q., et al. (2018). Revisiting slow slip events occurrence in Boso Peninsula, Japan, combining GPS data and repeating earthquakes analysis. *Journal of Geophysical Research: Solid Earth*, *123*(2), 1502–1515. https://doi.org/10.1002/2017jb014469

Geographical Survey Institute (GSI). (2008). Crustal movements in the Kanto district. *Report of the Coordinating Committee for Earthquake Prediction in Japanese*, *80*, 157–171.

Geological Survey of Japan, AIST (GSJ) & National Research Institute for Earth Science and Disaster Prevention (NIED). (2014). Short-term slow slip events in the Tokai area, the Kii Peninsula and the Shikoku District, Japan (from November 2013 to April 2013). *Report of the Coordinating Committee for Earthquake Prediction in Japanese*, *92*, 238–240.

Haines, J., Wallace, L. M., & Dimitrova, L. (2019). Slow slip event detection in Cascadia using vertical derivatives of horizontal stress rates. *Journal of Geophysical Research: Solid Earth*, *124*, 5153–5173. https://doi.org/10.1029/2018JB016898

Hawthorne, J. C., Simons, M., & Ampuero, J. P. (2016). Estimates of aseismic slip associated with small earthquakes near San Juan Bautista, CA. *Journal of Geophysical Research: Solid Earth*, *121*(11), 8254–8275. https://doi.org/10.1002/2016jb013120

Hirose, H., Hirahara, K., & Fujii, N. (2001). *Possible slow slip recurrence off Boso peninsula* (p. 140). Tokyo: Abstract of Fall Meeting Seismological Society of Japan. (in Japanese).

Hirose, H., Kimura, H., Enescu, B., & Aoi, S. (2012). Recurrent slow slip event likely hastened by the 2011 Tohoku earthquake. *Proceedings of the National Academy of Sciences of the United States of America*, *109*(38), 15157–15161. https://doi.org/10.1073/pnas.1202709109

Hirose, F., Nakajima, J., & Hasegawa, A. (2008). Three-dimensional velocity structure and configuration of the Philippine Sea slab beneath Kanto district, central Japan, estimated by double-difference tomography. *Journal of Seismological Society of Japan (Zisin)*, *2*(60), 123–138. https://doi.org/10.4294/zisin.60.123

Igarashi, T. (2020). Catalog of small repeating earthquakes for the Japanese Islands. *Earth Planets and Space*, *72*(1), 73. https://doi.org/10.1186/s40623-020-01205-2

Igarashi, T., Matsuzawa, T., & Hasegawa, A. (2003). Repeating earthquakes and interplate aseismic slip in the northeastern Japan subduction zone. *Journal of Geophysical Research*, *108*(B5), 2249. https://doi.org/10.1029/2002jb001920

Ikari, M. J., Marone, C., Saffer, D. M., & Kopf, A. J. (2013). Slip weakening as a mechanism for slow earthquakes. *Nature Geoscience*, *6*(6), 468–472. https://doi.org/10.1038/ngeo1818

Ishibashi, K. (1981). Specification of a soon-to-occur seismic faulting in the Tokai District, Central Japan, based upon seismotectonics. In D. W. Simpson, & P. G. Richards (Eds.), *Earthquake prediction*, (297–332). American Geophysical Union. https://doi.org/10.1029/ME004p0297

Ishida, M. (1992). Geometry and relative motion of the Philippine Sea Plate and Pacific Plate beneath the Kanto-Tokai District, Japan. *Journal of Geophysical Research*, *97*(B1), 489–513. https://doi.org/10.1029/91jb02567

Ito, Y., Hino, R., Kido, M., Fujimoto, H., Osada, Y., Inazu, D., et al. (2013). Episodic slow slip events in the Japan subduction zone before the 2011 Tohoku-Oki earthquake. *Tectonophysics*, *600*, 14–26. https://doi.org/10.1016/j.tecto.2012.08.022

Ito, Y., Obara, K., Shiomi, K., Sekine, S., & Hirose, H. (2007). Slow earthquakes coincident with episodic tremors and slow slip events. *Science*, *315*(5811), 503–506. https://doi.org/10.1126/science.1134454

Ito, A., Sugioka, H., Obana, K., Hino, R., Suetsugu, D., Nakahigashi, K., et al. (2017).Upper boundaries of the Pacific and Philippine Sea plates near the triple junction off the Boso Peninsula deduced from ocean-bottom seismic observations. *Earth Planets and Space*, *69*(1), 30. https://doi.org/10.1186/s40623-017-0608-4

Ito, A., Yamamoto, Y., Hino, R., Suetsugu, D., Sugioka, H., Nakano, M., et al. (2017). Tomographic image of crust and upper mantle off the Boso Peninsula using data from an ocean-bottom seismograph array. *Earth Planets and Space*, *69*(1), 118. https://doi.org/10.1186/s40623-017-0703-6

Kato, A., Igarashi, T., & Obara, K. (2014). Detection of a hidden Boso slow slip event immediately after the 2011 Mw 9.0 Tohoku-Oki earthquake. *Japan, Geophysical Research Letter*, *41*(16), 5868–5874. https://doi.org/10.1002/2014gl061053

Kawasaki, I., Asai, Y., & Tamura, Y. (2001). Space–time distribution of interplate moment release including slow earthquakes and the seismo-geodetic coupling in the Sanriku-oki region along the Japan trench. *Tectonophysics*, *330*(3–4), 267–283. https://doi.org/10.1016/s0040-1951(00)00245-6

Kobayashi, A., & Hirose, F. (2016). Aseismic slips synchronized with earthquakes in Northern Chiba prefecture, Central Japan. *Journal of Seismological Society of Japan (Zisin)*, *2*(69), 1–6. https://doi.org/10.4294/zisin.69.1

Liu, X., & Zhao, D. (2018). Upper and lower plate controls on the great 2011 Tohoku-oki earthquake. *Science Advances*, *4*(6), 1–7. https://doi.org/10.1126/sciadv.aat4396

Matsu'ura, M., & Hasegawa, Y. (1987). A maximum-likelihood approach to nonlinear inversion under constraints. *Physics of the Earth and Planetary Interiors*, *47*, 179–187. https://doi.org/10.1016/0031-9201(87)90076-8

Mazzotti, S., Henry, P., LePichon, X., & Sagiya, T. (1999). Strain partitioning in the zone of transition from Nankai subduction to Izu–Bonin collision (Central Japan): Implications for an extensional tear within the subducting slab. *Earth and Planetary Science Letters*, *172*(1–2), 1–10. https://doi.org/10.1016/s0012-821x(99)00189-2

Miyaoka, K., & Yokota, T. (2012). Development of stacking method for the detection of crustal deformation—Application to the early detection of slow slip phenomena on the plate boundary in the Tokai region using strain data. *Journal of Seismological Society of Japan (Zisin)*, *2*(65), 205–218. https://doi.org/10.4292/zisin.65.205

Nakajima, J., Hirose, F., & Hasegawa, A. (2009). Seismotectonics beneath the Tokyo metropolitan area, Japan: Effect of slab-slab contact and overlap on seismicity. *Journal of Geophysical Research*, *114*(B8), B08309. https://doi.org/10.1029/2008jb006101

Nakajima, J., & Hasegawa, A. (2016). Tremor activity inhibited by well-drained conditions above a megathrust. *Nature Communication*, *7*, 13863. https://doi.org/10.1038/ncomms13863

Nakajima, J., & Uchida, N. (2018). Repeated drainage from megathrusts during episodic slow slip. *Nature Geoscience*, *11*(5), 351–356. https://doi.org/10.1038/s41561-018-0090-z

National Research Institute for Earth Science and Disaster Prevention. (2010a). Recent continuous crustal tilt observation in the Kanto, Tokai, and northern Kii Peninsula Areas (November, 2009–April, 2010). *Report of the Coordinating Committee for Earthquake Prediction*, *84*, 147–151.(in Japanese).

National Research Institute for Earth Science and Disaster Prevention. (2010b). The earthquakes below the eastern coast of the Boso Peninsula in December 24, 2009. *Report of the Coordinating Committee for Earthquake Prediction*, *84*, 122–125.(in Japanese).

Nishikawa, T., & Ide, S. (2018). Recurring slow slip events and earthquake nucleation in the source region of the M7 Ibaraki-Oki earthquakes revealed by earthquake swarm and foreshock activity. *Journal of Geophysical Research: Solid Earth*, *123*(9), 7950–7968. https://doi.org/10.1029/2018jb015642

Nishikawa, T., Matsuzawa, T., Ohta, K., Uchida, N., Nishimura, T., & Ide, S. (2019). The slow earthquake spectrum in the Japan Trench illuminated by the S-net seafloor observatories. *Science*, *365*, 803–813. https://doi.org/10.1126/science.aax5618

Nishimura, T. (2014). Short-term slow slip events along the Ryukyu Trench, southwestern Japan, observed by continuous GNSS. *Progress in Earth and Planetary Sciences*, *1*(1), 22. https://doi.org/10.1186/s40645-014-0022-5

Nishimura, T., Matsuzawa, T., & Obara, K. (2013). Detection of short-term slow slip events along the Nankai Trough, southwest Japan, using GNSS data. *Journal of Geophysical Research: Solid Earth*, *118*(6), 3112–3125. https://doi.org/10.1002/jgrb.50222

Nishimura, T., Munekane, H., & Yarai, H. (2011). The 2011 off the Pacific coast of Tohoku Earthquake and its aftershocks observed by GEONET. *Earth Planets and Space*, *63*(7), 631–636. https://doi.org/10.5047/eps.2011.06.025

Nishimura, T., Ozawa, S., Murakami, M., Sagiya, T., Tada, T., Kaidzu, M., & Ukawa, M. (2001). Crustal Deformation caused by magma migration in the northern Izu Islands, Japan. *Geophysical Research Letters*, *28*(19), 3745–3748. https://doi.org/10.1029/2001GL013051

Nishimura, T., Yokota, Y., Tadokoro, K., & Ochi, T. (2018). Strain partitioning and interplate coupling along the northern margin of the Philippine Sea plate, estimated from Global Navigation Satellite System and Global Positioning System-Acoustic data. *Geosphere*, *14*(2), 535–551. https://doi.org/10.1130/ges01529.1

Obara, K. (2011). Characteristics and interactions between non-volcanic tremor and related slow earthquakes in the Nankai subduction zone, southwest Japan. *Journal of Geodynamics*, *52*(3–4), 229–248. https://doi.org/10.1016/j.jog.2011.04.002

Obara, K., & Hirose, H. (2006). Non-volcanic deep low-frequency tremors accompanying slow slips in the southwest Japan subduction zone. *Tectonophysics*, *417*(1–2), 33–51. https://doi.org/10.1016/j.tecto.2005.04.013

Obara, K., Tanaka, S., Maeda, T., & Matsuzawa, T. (2010). Depth-dependent activity of non-volcanic tremor in southwest Japan. *Geophysical Research Letters*, *37*, L13306. https://doi.org/10.1029/2010GL043679

Okada, Y. (1985). Surface deformation due to shear and tensile faults in a half-space. *Bulletin of the Seismological Society of America*, *75*(4), 1135–1154.

Okutani, T., & Ide, S. (2011). Statistic analysis of swarm activities around the Boso Peninsula, Japan: Slow slip events beneath Tokyo Bay? *Earth Planets and Space*, *63*(5), 419–426. https://doi.org/10.5047/eps.2011.02.010

Ozawa, S. (2017). Long-term slow slip events along the Nankai trough subduction zone after the 2011 Tohoku earthquake in Japan. *Earth Planets and Space*, *69*(1), 56. https://doi.org/10.1186/s40623-017-0640-4

Ozawa, S. W., Hatano, T., & Kame, N. (2019). Longer migration and spontaneous decay of aseismic slip pulse caused by fault roughness. *Geophysical Research Letters*, *46*(2), 636–643. https://doi.org/10.1029/2018gl081465

Ozawa, S., Nishimura, T., Munekane, H., Suito, H., Kobayashi, T., Tobita, M., & Imakiire, T. (2012). Preceding, coseismic, and postseismic slips of the 2011 Tohoku earthquake, Japan. *Journal of Geophysical Research*, *117*, B07404. https://doi.org/10.1029/2011JB009120

Pollitz, F., Nyst, M., Nishimura, T., & Thatcher, W. (2005). Coseismic slip distribution of the 1923 Kanto earthquake, Japan. *Journal of Geophysical Research*, *110*, B11408. https://doi.org/10.1029/2005JB003638

Radiguet, M., Perfettini, H., Cotte, N., Gualandi, A., Valette, B., Kostoglodov, V., et al. (2016). Triggering of the 2014 Mw7.3 Papanoa earthquake by a slow slip event in Guerrero, Mexico. *Nature Geoscience*, *9*(11), 829–833. https://doi.org/10.1038/ngeo2817

Rousset, B., Campillo, M., Lasserre, C., Frank, W. B., Cotte, N., Walpersdorf, A., et al. (2017). A geodetic matched filter search for slow slip with application to the Mexico subduction zone. *Journal of Geophysical Research: Solid Earth*, *122*(12), 10498–10514. https://doi.org/10.1002/2017jb014448

Saffer, D. M., & Wallace, L. M. (2015). The frictional, hydrologic, metamorphic and thermal habitat of shallow slow earthquakes. *Nature Geoscience*, *8*(8), 594–600. https://doi.org/10.1038/ngeo2490

Sagiya, T. (2004). Interplate coupling in the Kanto District, Central Japan, and the Boso Peninsula silent earthquake in May 1996. *Pure and Applied Geophysics*, *161*(11–12), 2327–2342. https://doi.org/10.1007/s00024-004-2566-6

Schwartz, S. Y., & Rokosky, J. M. (2007). Slow slip events and seismic tremor at circum-Pacific subduction zones. *Review of Geophysics*, *45*, RG3004. https://doi.org/10.1029/2006RG000208

Sekine, S., Hirose, H., & Obara, K. (2010). Along-strike variations in short-term slow slip events in the southwest Japan subduction zone. *Journal of Geophysical Research*, *115*, B00A27. https://doi.org/10.1029/2008jb006059

Suito, H., Nishimura, T., Tobita, M., Imakiire, T., & Ozawa, S. (2011). Interplate fault slip along the Japan Trench before the occurrence of the 2011 off the Pacific coast of Tohoku Earthquake as inferred from GPS data. *Earth Planets and Space*, *63*(7), 615–619. https://doi.org/10.5047/eps.2011.06.053

Suito, H., & Ozawa, S. (2009). Transient crustal deformation in the Tokai district – The Tokai slow slip event and postseismic deformation caused by the 2004 off southeast Kii Peninsula earthquake. *Journal of Seismological Society of Japan (Zisin)*, *2*(61), 113–135. https://doi.org/10.4294/zisin.61.113

Takagi, R., Uchida, N., & Obara, K. (2019). Along strike variation and migration of long-term slow slip events in the western Nankai subduction zone, Japan. *Journal of Geophysical Research: Solid Earth*, *124*(4), 3853–3880 https://doi.org/10.1029/2018jb016738

Toda, S., Lin, J., & Stein, R. S. (2011). Using the 2011 Mw 9.0 off the Pacific coast of Tohoku Earthquake to test the Coulomb stress triggering hypothesis and to calculate faults brought closer to failure. *Earth Planets and Space*, *63*, 39. https://doi.org/10.5047/eps.2011.05.010

Vallée, M., Nocquet, J. M., Battaglia, J., Font, Y., Segovia, M., Régnier, M., et al. (2013). Intense interface seismicity triggered by a shallow slow slip event in the Central Ecuador subduction zone. *Journal of Geophysical Research: Solid Earth*, *118*(6), 2965–2981. https://doi.org/10.1002/jgrb.50216

Wada, I., & He, J. (2017). Thermal structure of the Kanto region, Japan. *Geophysical Research Letters*, *44*, 7194–7202. https://doi.org/10.1002/2017GL073597

Wallace, L. M. (2020). Slow slip events in New Zealand. *Annual Review of Earth and Planetary Sciences*, *48*(1), 175–203. https://doi.org/10.1146/annurev-earth-071719-055104

Wdowinski, S., Bock, Y., Zhang, J., Fang, P., & Genrich, J. (1997). Southern California permanent GPS geodetic array: Spatial filtering of daily positions for estimating coseismic and postseismic displacements induced by the 1992 Landers earthquake. *Journal of Geophysical Research: Solid Earth*, *102*(B8), 18057–18070. https://doi.org/10.1029/97jb01378

Wech, A. G., Creager, K. C., & Melbourne, T. I. (2009). Seismic and geodetic constraints on Cascadia slow slip. *Journal of Geophysical Research*, *114*, B10316. https://doi.org/10.1029/2008JB006090

Wessel, P., Smith, W. H. F., Scharroo, R., Luis, J., & Wobbe, F. (2013). Generic mapping tools: Improved version released. *EOS Transactions American Geophysical Union*, *94*(45), 409–410. https://doi.org/10.1002/2013EO450001

Yanagisawa, H., Goto, K., Sugawara, D., Kanamaru, K., Iwamoto, N., & Takamori, Y. (2016). Tsunami earthquake can occur elsewhere along the Japan Trench—Historical and geological evidence for the 1677 earthquake and tsunami. *Journal of Geophysical Research: Solid Earth*, *121*(5), 3504–3516. https://doi.org/10.1002/2015jb012617

Yarai, H., & Ozawa, S. (2013). Quasi-periodic slow slip events in the afterslip area of the 1996 Hyuga-nada earthquakes, Japan. *Journal of Geophysical Research: Solid Earth*, *118*(5), 2512–2527. https://doi.org/10.1002/jgrb.50161